J|A|C|S
ARTICLES
Published on Web 08/19/2005

19-Electron Intermediates and Cage-Effects in the Photochemical Disproportionation of $[CpW(CO)_3]_2$ with Lewis Bases

James F. Cahoon,[†] Matthias F. Kling,[†,‡] Stefan Schmatz,[§] and Charles B. Harris*[,†]

Contribution from the Department of Chemistry, University of California, Berkeley, California 94720, and Chemical Sciences Division, Lawrence Berkeley National Laboratory, Berkeley, California 94720, and Institut für Physikalische Chemie, Universität Göttingen, Tammannstr. 6, 37077 Göttingen, Germany

Received April 6, 2005; E-mail: cbharris@berkeley.edu

Abstract: The role of 19-electron intermediates in the photochemical disproportionation of $[CpW(CO)_3]_2$ ($Cp = C_5H_5$) with Lewis bases (PR_3; R = OMe, Bu, Ph) is investigated on the ultrafast time scale using femtosecond VIS-pump, IR-probe spectroscopy. Formation of a 19-electron (19e) species $CpW(CO)_3PR_3^{\bullet}$ by coordination of PR_3 with photogenerated 17-electron (17e) radicals $CpW(CO)_3^{\bullet}$ is directly observed, and equilibrium is established between the 17e radicals and the 19e intermediates favoring 19e intermediates in the order: Bu > OMe ≫ Ph. Steric effects dominate the 17e/19e equilibrium when the cone-angle of the Lewis base exceeds a certain limiting value (between 132° and 145°), but below this value electronic properties of the Lewis base control the 17e/19e dynamics. Disproportionation occurs in less than 200 picoseconds by electron transfer between a solvent caged 17e radical and 19e, highly reducing species. The rate and extent of ultrafast disproportionation depends on both the identity and concentration of the Lewis base. In low concentrations of PR_3 (typically 1−2 M or less) or with Lewis bases whose equilibrium heavily favors 17e radicals (e.g., PPh_3), disproportionation is rate-limited by breakdown of the solvent cage. Density functional theory calculations on vibrational frequencies and charge distributions of the various complexes support the experimental results.

I. Introduction

The 18-electron rule, one of the fundamental concepts in organometallic chemistry, predicts the greatest stability in compounds with an even number of electrons, yet the existence of odd-electron compounds both as stable species and intermediates in catalytic processes has long been recognized.[1,2] In addition to electron deficient 17-electron (17e) radicals, 19-electron (19e) species have been identified as potential intermediates in a variety of catalytic and electron-transfer reactions.[1,2] One of the first 19e complexes, cobaltocene, was synthesized as early as 1953,[3] and many stable 19e complexes have subsequently been characterized.[4−6] While these complexes formally contain 19 valence electrons, the '19th' electron is commonly localized on a ligand, allowing the metal to retain an effective 18-electron count. As a result, 19e compounds are often more accurately referred to as 18+δ-electron complexes, where the value of δ reflects the degree of electron density residing on the metal center.

Although 18+δ complexes are well characterized, a different class of less stable, "true" 19e complexes have been postulated as intermediates in organometallic reactions.[1,2,7] Since "true" 19e species are highly reactive, characterization has only been possible in rare instances. For example, $Mn(CO)_5Cl^-$ was generated by γ-irradiation of $Mn(CO)_5Cl$, studied both computationally[8] and experimentally[9] and found to be better described as a 19 rather than 18+δ-electron complex. In condensed phase organometallic chemistry, however, 19e species are, in general, generated by coordination of a 2-electron donor with a 17e radical

$$ML_n^{\bullet}\ (17e) + PR_3 \rightleftharpoons ML_n\,PR_3^{\bullet}\ (19e)$$

$$ML_n = CpMo(CO)_3^{\bullet},\ CpW(CO)_3^{\bullet},\ CpFe(CO)_2^{\bullet},\ Mn(CO)_5^{\bullet},\ \text{etc.}$$

In some instances, the 19e intermediate is predicted to be

[†] University of California, Berkeley.
[‡] Present address: FOM Institute for Atomic and Molecular Physics (AMOLF), Kruislaan 407, 1098 SJ Amsterdam, The Netherlands.
[§] Universität Göttingen.

(1) Baird, M. C. *Chem. Rev.* **1988**, *88*, 1217−1227.
(2) Astruc, D. *Chem. Rev.* **1988**, *88*, 1189−1216; Tyler, D. R. *Acc. Chem. Res.* **1991**, *24*, 325−331.
(3) Wilkinson, G. *J. Am. Chem. Soc.* **1952**, *74*, 6148−6149; Pfab, W.; Fischer, E. O. *Anorg. Allg. Chem.* **1953**, *274*, 316−322.
(4) Mao, F.; Philbin, C. E.; Weakley, T. J. R.; Tyler, D. R. *Organometallics* **1990**, *9*, 1510−1516. Mao, F.; Sur, S. K.; Tyler, D. R. *Organometallics* **1991**, *10*, 419−423.
(5) Meyer, R.; Schut, D. M.; Keana, K. J.; Tyler, D. R. *Inorg. Chim. Acta* **1995**, *240*, 405−412.
(6) Schut, D. M.; Keana, K. J.; Tyler, D. R.; Rieger, P. H. *J. Am. Chem. Soc.* **1995**, *117*, 8939−8946.
(7) Geiger, W. E. *Acc. Chem. Res.* **1995**, *28*, 351−357.
(8) Braden, D. A.; Tyler, D. R. *Organometallics* **1998**, *17*, 4060−4064.
(9) Anderson, O. P.; Fieldhouse, S. A.; Forbes, C. E.; Symons, M. C. R. *J. Chem. Soc., Dalton Trans.* **1976**, 1329−1336. Lionel, T.; R., M. J.; Preston, K. F., *Chem. Phys. Lett.* **1981**, *81*, 17−20.

Scheme 1. Photochemical Disproportionation Mechanism for $[CpM(CO)_3]_2$ (M = Cr, Mo, W) in Lewis Bases PR_3 (R = alkyl, alkoxy, aryl, aryloxy) as Proposed by Tyler[14,15a]

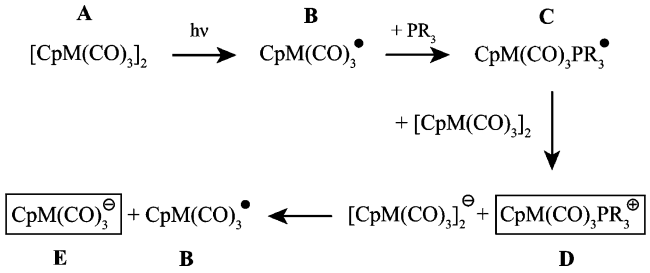

[a] Final disproportionated products are enclosed in boxes.

thermodynamically favorable with respect to the 17e species, yet unstable with respect to 18e counterparts.[10] These "true" 19e species are hence postulated as highly reactive, short-lived intermediates leading to stable even-electron products. Strong indirect evidence supports the formation of such species,[11−15] but experimental limitations previously hindered the direct observation of these intermediates and their reactions. Using transient IR spectroscopy with femtosecond time resolution, we directly observe the formation of 19e intermediates and investigate the dynamics of these short-lived species in the disproportionation of $[CpW(CO)_3]_2$ with Lewis bases.

The disproportionation of $[CpM(CO)_3]_2$ (M = Cr, Mo, W) into $CpM(CO)_3^-$ and $CpM(CO)_3L^+$ (L = phosphine or phosphite) has been well-investigated and was one of the earliest photochemical reactions postulated to involve a 19e intermediate.[13−15] The currently accepted mechanism for this reaction, proposed by Tyler and co-workers,[14,15] is depicted in Scheme 1. Photoexcitation of $[CpM(CO)_3]_2$ (**A**) at visible wavelengths leads to M−M bond cleavage and the formation of two 17e radicals $CpM(CO)_3^\bullet$ (**B**). In the presence of Lewis bases PR_3 (R = alkyl, alkoxy, aryl, or aryloxy), a highly reducing 19e species $CpM(CO)_3PR_3^\bullet$ (**C**) is formed. Disproportionation is initiated by this 19e species: electron transfer from $CpM(CO)_3PR_3^\bullet$ (**C**) to $[CpM(CO)_3]_2$ (**A**) leads to formation of the cationic disproportionated product $CpM(CO)_3PR_3^+$ (**D**) and a negatively charged parent dimer $[CpM(CO)_3]_2^-$; successive M−M bond rupture of the negatively charged dimer yields a 17e radical $CpW(CO)_3^\bullet$ (**B**) and the anionic disproportionated product $CpW(CO)_3^-$ (**E**). Evidence for this mechanism includes quantum yield measurements of varying values greater than unity which are consistent with the radical chain process in Scheme 1 and the occurrence of disproportionation when the negatively charged dimer was produced by Na metal reduction.[14]

Scott et al. also found evidence for the formation of a 19e species while studying the electron-transfer reactions of photogenerated $CpW(CO)_3^\bullet$ radicals.[12] The rate of reduction of ferrocenium ions and benzoquinone by the $CpW(CO)_3^\bullet$ radical was found to depend linearly upon the concentration of PPh_3, and this dependence was attributed to the formation of $CpW(CO)_3PPh_3^\bullet$, the same 19e species proposed by Tyler.

Scheme 2. Mechanism of Ultrafast Disproportionation[a]

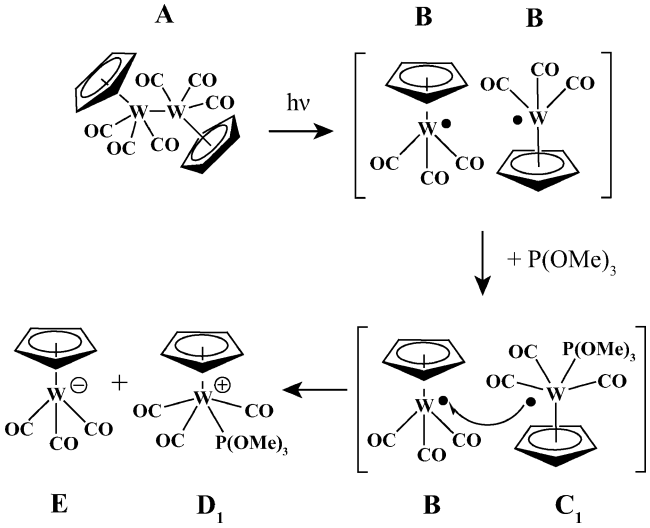

[a] Brackets represent the solvent cage.

We recently communicated our preliminary results on the photochemistry of $[CpW(CO)_3]_2$ in the Lewis base $P(OMe)_3$ and directly monitored the formation of a 19e species by coordination of the Lewis base $P(OMe)_3$ with the 17e radical $CpW(CO)_3^\bullet$.[16] We observed the formation of disproportionated products on a picosecond time scale and proposed a new mechanism for ultrafast disproportionation, as shown in Scheme 2. Homolysis of the dimer (**A**) produces two 17e radicals (**B**) enclosed by a cage of solvent molecules, represented by brackets in Scheme 2. Coordination of $P(OMe)_3$ generates a 19e intermediate ($\mathbf{C_1}$) which can transfer an electron to the 17e radical (**B**) while the two are in close proximity, forming the final disproportionated products ($\mathbf{D_1}$, **E**). Diffusional motion eventually separates the radical species, precluding charge transfer.

In this paper, we report detailed studies on the disproportionation reaction of $[CpW(CO)_3]_2$ in three Lewis bases (PR_3; R = OMe, Bu, Ph). These particular Lewis bases were chosen for their different electron-donating ability and cone-angle, enabling us to investigate electronic and steric effects on the reactivity of 19e intermediates. Using femtosecond VIS-pump, IR-probe spectroscopy we are able to resolve the complex dynamics and cage-effects involved in disproportionation and formation of 19e intermediates on an ultrafast time scale.

The paper is organized as follows: Section II provides a brief account of our experimental techniques and theoretical approach. Section III presents the time-resolved results of pump−probe experiments, discusses the principal reaction mechanisms, and addresses the influence of particular Lewis bases on the disproportionation kinetics. Our conclusions are summarized in Section IV.

II. Methods

A. Samples. $[CpW(CO)_3]_2$, trimethyl phosphite ($P(OMe)_3$), *n*-tributylphosphine (PBu_3), and triphenylphosphine (PPh_3) were obtained

(10) Philbin, C. E.; Granatir, C. A.; Tyler, D. R., *Inorg. Chem.* **1986**, *25*, 4806−4807. Therien, M. J.; Trogler, W. C., *J. Am. Chem. Soc.* **1987**, *109*, 5127−5133. Zhang, Y.; Gosser, D. K.; Rieger, P. H.; Sweigart, D. A. *J. Am. Chem. Soc.* **1991**, *113*, 4062−4068.
(11) Castellani, M. P.; Tyler, D. R. *Organometallics* **1989**, *8*, 2113−2120; Dixon, A. J.; George, M. W.; Hughes, C.; Poliakoff, M.; Turner, J. J. *J. Am. Chem. Soc.* **1992**, *114*, 1719−1729. Lin, Z.; Hall, M. B. *J. Am. Chem. Soc.* **1992**, *114*, 6574−6575. Neto, C. C.; Kim, S.; Meng, Q.; Sweigart, D. A.; Chung, Y. K. *J. Am. Chem. Soc.* **1993**, *115*, 2077−2078. Stiegman, A. E.; Goldman, A. S.; Philbin, C. E.; Tyler, D. R. *Inorg. Chem.* **1986**, *25*, 2976−2979.
(12) Scott, S. L.; Espenson, J. H.; Chen, W.-J. *Organometallics* **1993**, *12*, 4077−4084.
(13) Stiegman, A. E.; Tyler, D. R. *J. Am. Chem. Soc.* **1982**, *104*, 2944−2945. Stiegman, A. E.; Tyler, D. R. *Coord. Chem. Rev.* **1985**, *63*, 217−240.
(14) Stiegman, A. E.; Stieglitz, M.; Tyler, D. R. *J. Am. Chem. Soc.* **1983**, *105*, 6032−6037.
(15) Philbin, C. E.; Goldman, A. S.; Tyler, D. R. *Inorg. Chem.* **1986**, *25*, 4434−4436.
(16) Kling, M. F.; Cahoon, J. F.; Glascoe, E. A.; Shanoski, J. E.; Harris, C. B. *J. Am. Chem. Soc.* **2004**, *126*, 11414−11415.

from Aldrich, Inc. and spectroscopic grade CH_2Cl_2 was purchased from EMD Chemicals. All samples were used without further purification. Air sensitive materials were stored and handled under nitrogen atmosphere in a glovebox (Vacuum Atmospheres Company). Air and light-sensitive solutions were continuously purged with argon and rigorously secluded from all ambient light sources.

B. Femtosecond Infrared Spectroscopy. The experimental apparatus has been described in detail elsewhere.[17] In brief, the setup consists of a Ti:sapphire regenerative amplifier (SpectraPhysics, Spitfire) seeded by a Ti:sapphire oscillator (SpectraPhysics, Tsunami) to produce a 1 kHz pulse train of 100 fs pulses centered at 800 nm with an average pulse energy of 0.9 mJ. The output of this system is split, with one part used for harmonic generation of 400 nm pump pulses and the second to deliver tunable mid-IR probe pulses from a home-built optical parametric amplifier (OPA). The maximum energy of generated 400 nm light is 40 μJ, but can be reduced to smaller energies when required by specific experimental consideration (typically between 5 and 10 μJ were used in the current investigation to avoid multiphoton absorption). Infrared pulses tunable from 3.0 to 6.0 μm with a spectral width of ca. 200 cm^{-1} and pulse durations around 100 fs are routinely generated. The IR probe beam is split after the OPA into signal and reference lines using a 50% germanium beam splitter. The signal line and pump beam are overlapped at the sample and focused using CaF_2 lenses to provide a diameter at the sample of 100 μm and 200 μm, respectively. The sample, under Ar atmosphere, is flowed using a mechanical pump through a cell (Harrick Scientific) fitted with 1.5 mm thick CaF_2 or MgF_2 windows, giving an optical path length of 390 μm. Sample concentrations are adjusted so that the optical density (OD) of the sample at the pump wavelength is ca. OD = 1. Using a silica wafer, the pump and signal beams are cross-correlated to identify time zero and a time resolution of 150 to 200 fs is generally determined. The reference and signal IR beams are sent along a parallel path through a computer controlled spectrograph (Acton Research Corporation, SpectraPro-150) with entrance slits routinely set at 50 μm to achieve a spectral resolution of ca. 3 cm^{-1}. Spectrally dispersed signal and reference beams are detected by a 2 × 32 element MCT-array IR detector (Infrared Associates, Inc.) using a high-speed signal acquisition system and data acquisition software (Infrared Systems Development Corp.). Differences in optical density (ΔOD) as small as $\Delta OD = 5 \cdot 10^{-5}$ can be observed in the experiment.

C. Data Analysis. Kinetic data were derived from the spectral data taken at numerous picosecond pump−probe delay times. The absorbance values within distinct spectral ranges[18] for the various chemical species were averaged at each individual time delay. The kinetics for each species were then fit to one or more exponentials convoluted with a Gaussian (150 fs fwhm) to account for limited time resolution and accurately reflect the instrument response function. All reported errors correspond to 95% confidence intervals. Where noted, Gaussian peak fitting to the spectral data was performed to separate the contributions from two spectrally overlapped peaks, and kinetics were derived from the areas of the Gaussians.

D. Theoretical. Density functional theory (DFT) calculations have been performed to assist in the characterization of the various intermediate species and to facilitate an understanding of the dynamical behavior. Density functionals of the type used in this work have been shown to yield reliable results in calculations for transition-metal complexes.[19]

The DFT calculations were carried out using the program package Gaussian03,[20] and the B3LYP hybrid method[21] was used in all calculations. It is composed of Becke's three-parameter exchange-functional[22] and the Lee−Yang−Parr nonlocal correlation functional.[23] Generic basis sets used consisted of the double-ζ LANL2DZ in conjunction with the relativistic effective core potential (ECP) of Hay and Wadt[24] for tungsten and 6-31G(d) (**I**), 6-31G+(d) (**II**), and 6-311+G(d,p) (**III**) basis sets for all other atoms. The Hessian matrices were calculated at the stationary points in order to ensure that true minima on the potential energy hypersurfaces had been found. Harmonic vibrational frequencies, appropriately scaled, are used in the spectral analysis of the experimental data.

In addition, single point calculations on the optimized geometries were carried out making use of the Stuttgart effective core potential ECP60MDF[25] for tungsten with the associated basis set (8s7p6d) → [6s5p3d] plus an additional *f* polarization[26] in conjunction with basis **II**, resulting in more than 800 contracted Gaussian-type orbitals for the largest complex. Natural bond orbital (NBO) analysis[27] has been performed wherefrom natural atomic charges were derived.

III. Results and Discussion

A. Reactions in CH_2Cl_2. The photochemistry of $[CpW(CO)_3]_2$ was monitored in the solvent CH_2Cl_2, and photolysis at 400 nm was found to yield only 17e radicals $CpW(CO)_3^{\bullet}$. Time-resolved transient difference spectra after 400 nm photolysis of an approximately 1 mM solution of $[CpW(CO)_3]_2$ in neat CH_2Cl_2 are shown in Figure 1a. Negative absorbances result from the depletion of the parent molecule $[CpW(CO)_3]_2$ (**A**) while positive absorptions result from the formation of new species following laser photolysis. Two strong parent bleaches for *anti*-$[CpW(CO)_3]_2$ (**A**) are observed at 1909 and 1956 cm^{-1}, originating from the two b_u and one a_u carbonyl stretching modes of *anti*-$[CpW(CO)_3]_2$, the most stable isomer in nonpolar and weakly polar solutions.[28] A negligible contribution from the gauche-isomer is observed by the weak bleach at 2012 cm^{-1}. The 17e $CpW(CO)_3^{\bullet}$ radicals (**B**) exhibit transient absorptions at 1880 and 1995 cm^{-1}.[28] Note that the radical function results in a larger splitting between the carbonyl modes in comparison to the parent species.

Photolysis of $[CpW(CO)_3]_2$ can result in carbonyl loss with shorter excitation wavelengths; however, no significant absorption attributable to $Cp_2W_2(CO)_5$ is observed in this experiment. $[CpW(CO)_3]_2$ possesses two band maxima in the UV/Visible region at 493 and 362 nm in CCl_4, corresponding to a weak $d\pi \rightarrow \sigma^*$ transition and a strong $\sigma \rightarrow \sigma^*$ transition, respectively.[29] High energy excitation results in greater carbonyl loss while excitation into the lower energy band suppresses the carbonyl-loss pathway. In this experiment, excitation (400 nm) occurs between the two band maxima and is sufficiently low in energy to suppress a carbonyl-loss pathway. If carbonyl-loss products are generated by photolysis at 400 nm, then the products are in such a low yield as to be undetectable by our experimental apparatus. Significant formation of carbonyl-loss products would be expected with higher excitation energies. Photolysis of $[CpW(CO)_3]_2$ may also result in halogen atom abstraction by the 17e

(17) Shanoski, J. E.; Payne, C. K.; Kling, M. F.; Glascoe, E. A.; Harris, C. B. *Organometallics* **2005**, *24*, 1852−1859.
(18) Spectral ranges are as follows: $CpW(CO)_3$ 1870−1878 cm^{-1}; $CpW(CO)_3PR_3$ 1830−1850 cm^{-1} (R═OMe), 1820−1850 cm^{-1} (R═Bu); $CpW(CO)_3^-$ 1750−1760 cm^{-1}; $CpW(CO)_2PR_3^+$ 2059−2070 cm^{-1} (R═OMe), 2038−2052 cm^{-1} (R═Bu), 2048−2061 cm^{-1} (R═Ph).
(19) Niu, S.; Hall, M. B. *Chem. Rev.* **2000**, *100*, 353−405.
(20) Frisch, M. J.; et al. Gaussian03, Revision B.04; Gaussian, Inc.: Wallingford CT, 2004.
(21) Stephens, P. J.; Devlin, G. J.; Chabalowski, C. F.; Frisch, M. M. *J. Phys. Chem.* **1994**, *98*, 11623−11627.
(22) Becke, A. D. *J. Chem. Phys.* **1993**, *98*, 5648−5652.
(23) Lee, C.; Yang, W.; Parr, R. G. *Phys. Rev. B* **1988**, *37*, 785−789.
(24) Hay, P. J.; Wadt, W. R. *J. Chem. Phys.* **1985**, *82*, 299−310.
(25) Andrae, D.; Häussermann, U.; Dolg, M.; Stoll, H.; Preuss, H. *Theor. Chim. Acta* **1990**, *77*, 123−141.
(26) Cahoon, J. F.; Kling, M. F.; Harris, C. B.; Schmatz, S., manuscript in preparation.
(27) Reed, E. A.; Curtiss, L. A.; Weinhold, F. *Chem. Rev.* **1988**, *88*, 899−926.
(28) Virrels, I. G.; George, M. W.; Johnson, F. P. A.; Turner, J. J.; Westwell, J. R. *Organometallics* **1995**, *14*, 5203−5208. Peters, J.; George, M. W.; Turner, J. J. *Organometallics* **1995**, *14*, 1503−1506.
(29) Bitterwolf, T. E., *Coord. Chem. Rev.* **2001**, *211*, 235−254.

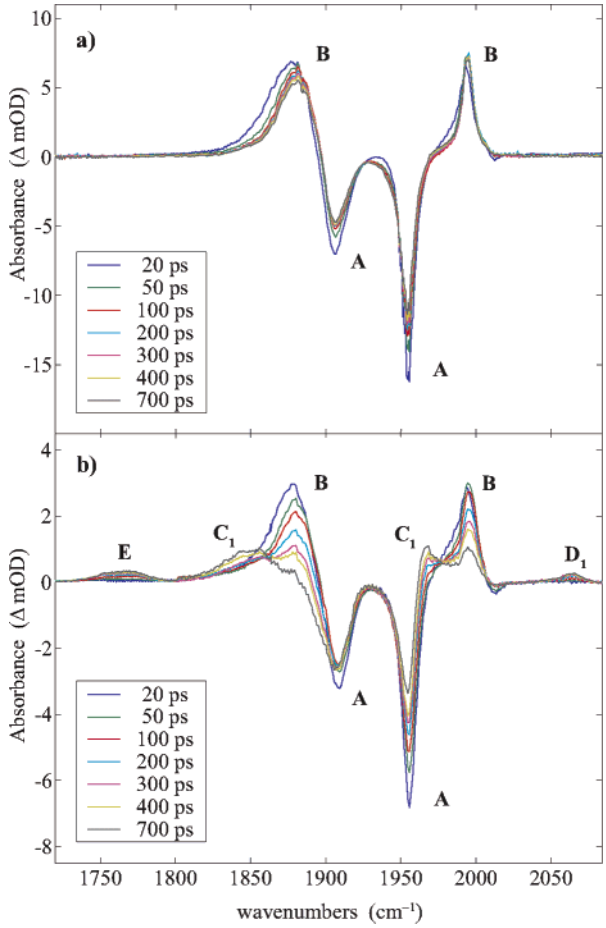

Figure 1. Spectral data recorded for $[CpW(CO)_3]_2$ in (a) neat CH_2Cl_2 and (b) 1.6 M $P(OMe)_3$ with CH_2Cl_2.

radical $CpW(CO)_3^\bullet$ in the presence of organic halides such as CCl_4.[30] In the present study, CH_2Cl_2 is used as the solvent due to the high solubility of $[CpW(CO)_3]_2$, phosphines, and phosphites in this solvent. In comparison to CCl_4, chlorine atom abstraction is unfavorable in CH_2Cl_2, with a second-order rate constant $k < 0.6\ M^{-1}s^{-1}$, 4 orders of magnitude lower than in CCl_4 ($k = 1.3 \pm 0.2 \times 10^4\ M^{-1}s^{-1}$).[30] Chlorine atom abstraction would occur only to a limited extent and on a time scale of milliseconds or greater. Accordingly, no evidence for chlorine abstraction in CH_2Cl_2 was observed in our experiments on the ultrafast time scale.

In neat CH_2Cl_2, 17e radicals (**B**) exhibit only vibrational relaxation and geminate recombination, leading to a decay of 5% within ca. 50 ps, but show no further decay on longer time scales. Geminate recombination of the 17e radicals results in formation of $[CpW(CO)_3]_2$ and recovery of the bleaches for the dimer (labeled **A** in Figure 1). See the Supporting Information for a more detailed discussion of the geminate recombination kinetics.

B. Reactions with $P(OMe)_3$. The addition of the strong Lewis base $P(OMe)_3$ to CH_2Cl_2 dramatically changes the intermediates and products on the ultrafast time scale, as shown by a comparison of Figures 1a and 1b. Time-resolved difference spectra after photolysis of $[CpW(CO)_3]_2$ in a 1.6 M solution of $P(OMe)_3$ in CH_2Cl_2 ("phosphite solution") are shown in Figure 1b. In neat CH_2Cl_2, no significant decay of the 17e radicals (**B**) occurs after 50 ps, but in phosphite solution near complete decay of the radical is observed and four additional peaks can be seen, centered at 1770, 1850, 1967, and 2064 cm^{-1}, that are assigned to the anionic disproportionated product $CpW(CO)_3^-$ (**E**), two peaks of the 19e intermediate $CpW(CO)_3P(OMe)_3^\bullet$ ($\mathbf{C_1}$), and the cationic disproportionated product $CpW(CO)_3P(OMe)_3^+$ ($\mathbf{D_1}$), respectively. Assignments are based on literature data, comparison to analogous compounds containing Mo rather than W,[28,31] and extensive DFT calculations (see Table 1).

Neglecting the spectral trace at 20 ps, which shows effects of peak broadening due to vibrational excitation after photolysis, isosbestic points at 1865 cm^{-1} and 1978 cm^{-1} in Figure 1b indicate that the 19e intermediate ($\mathbf{C_1}$) is directly formed from the 17e radical (**B**)

$$CpW(CO)_3^\bullet\,(\mathbf{B}) + P(OMe)_3 \rightleftharpoons CpW(CO)_3P(OMe)_3^\bullet\,(\mathbf{C_1}).$$

Fits to the kinetic data support this conclusion and are shown in Figure 2a. Kinetics for the 19e intermediate ($\mathbf{C_1}$) were fit to an exponential decay and exponential rise, yielding 12 ± 2 ps ($\tau = k^{-1}$) and 464 ± 101 ps respectively,[32] with the exponential decay attributed to spectral overlap with the vibrationally hot 17e radical which cools on this time scale and the exponential rise attributed to the actual rise of the 19e intermediate.[33] Kinetics for the 17e radical (**B**) were fit to two exponential decays giving 40 ± 4 ps and 417 ± 17 ps. The fast decay results from a combination of vibrational relaxation, disproportionation (as explained below), and geminate recombination. As in neat

Table 1. Calculated and Observed Vibrational Frequencies (in cm^{-1}) of Relevant Species for the Photochemistry of $[CpW(CO)_3]_2$ with PR_3 (R= OMe, Bu, Ph) in CH_2Cl_2[a]

	calculated	observed
anti-$[CpW(CO)_3]_2$ (**A**)	1892 (0.0), 1915 (0.2), 1924 (0.8), 1932 (0.0), 1968 (1.0), 2000 (0.0)[b]	1909 (s), 1956 (s)
gauche-$[CpW(CO)_3]_2$	1902 (0.2), 1909 (0.3), 1937 (0.4), 1944 (0.0), 1970 (0.6), 2014 (0.4)[b]	2012 (w)
anti-$[CpW(CO)_3]_2^-$	1839 (0.1), 1869 (0.8), 1881 (1.9)[b]	not observed
$CpW(CO)_3^\bullet$ (17e, **B**)	1906 (0.6), 1907 (0.4), 1989 (0.3)[d]	1880 (s), 1995 (s)
$CpW(CO)_3^-$ (18e, **E**)	1783 (0.7), 1784 (0.7), 1879 (0.4)[d]	1770 (w)
$CpW(CO)_3P(OMe)_3^\bullet$ (19e, $\mathbf{C_1}$)	1867 (0.5), 1877 (0.4), 1961 (0.4)[c]	1850 (s), 1967 (m)
$CpW(CO)_3P(OMe)_3^+$ (18e, $\mathbf{D_1}$)	1976 (0.5), 2000 (0.2), 2056 (0.3)[c]	1995 (w), 2064 (w)
$CpW(CO)_3PBu_3^\bullet$ (19e, $\mathbf{C_2}$)	1821(0.8), 1857 (0.2), 1937 (0.3)[c]	1836 (m), 1943 (w)
$CpW(CO)_3PBu_3^+$ (18e, $\mathbf{D_2}$)	1952 (0.5), 1978 (0.2), 2039 (0.3)[c]	2044 (w)
$CpW(CO)_3PPh_3^\bullet$ (19e, $\mathbf{C_3}$)	1844 (0.7), 1864 (0.2), 1947 (0.3)[c]	1850(w)
$CpW(CO)_3PPh_3^+$ (18e, $\mathbf{D_3}$)	1965 (0.5), 1981 (0.2), 2040 (0.3)[c]	2054 (w)

[a] Calculated frequencies are scaled by the factor 0.9614[34] [b] Basis set **I**. [c] Basis set **II**. [d] Basis set **III**; relative intensities are given in parentheses (*w* = weak, m = medium, s = strong; calculated intensities are normalized with respect to the 1968 cm^{-1} mode of *anti*-$[CpW(CO)_3]_2$); except for the last four entries in the table, observed frequencies are given for phosphite solutions.

(30) Laine, R. M.; Ford, P. C. *Inorg. Chem.* **1977**, *16*, 388−391. Scott, S. L.; Espenson, J. H.; Zhu, Z. *J. Am. Chem. Soc.* **1993**, *115*, 1789−1797. Song, J.-S.; Bullock, R. M.; Creutz, C. *J. Am. Chem. Soc.* **1991**, *113*, 9862−9864.

(31) Haines, R. J.; Nyholm, R. S.; Stiddard, M. H. B. *J. Chem. Soc. A.* **1968**, 43−46. Haines, R. J.; Nolte, C. R. *J. Organometallic Chem.* **1970**, *24*, 725−736. Haines, R. J.; DuPreez, A. L.; Marais, I. L. *J. Organomet. Chem.* **1971**, *28*, 97−104. Allen, D. M.; Cox, A.; Kemp, T. J.; Sultana, Q.; Pitts, R. B. *J. Chem. Soc., Dalton Trans.* **1976**, 1189−1193. Baker, M. L.; Bloyce, P. E.; Campen, A. K.; Rest, A. J. *J. Chem. Soc., Dalton Trans.* **1990**, 2825−2832.

(32) Errors correspond to 95% confidence intervals. Large errors result from spectral overlap with the 17e radical peak.

Scheme 3. Reactions of $[CpW(CO)_3]_2$ with $P(OMe)_3$[a]

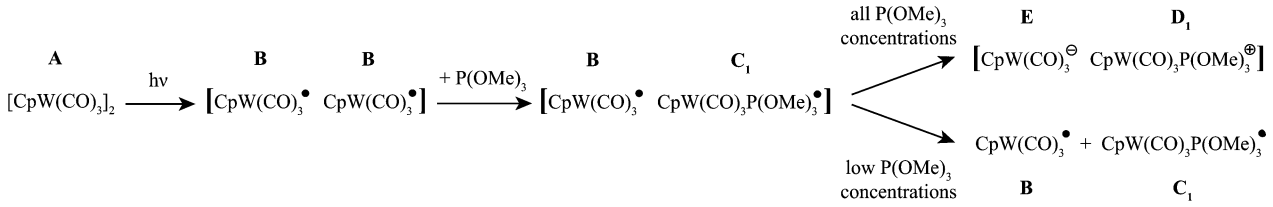

[a] Brackets represent the solvent cage.

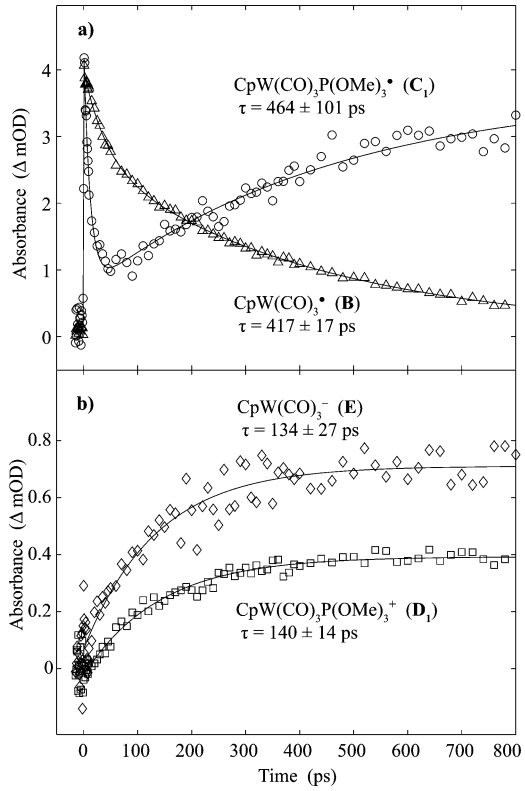

Figure 2. Kinetic plots for (a) $CpW(CO)_3P(OMe)_3^{\bullet}$ and $CpW(CO)_3^{\bullet}$, and (b) $CpW(CO)_3^-$ and $CpW(CO)_3P(OMe)_3^+$ following 400 nm photolysis of $[CpW(CO)_3]_2$ in a 1.6 M solution of $P(OMe)_3$ with CH_2Cl_2. Lines represent fits to the data (see text).

CH_2Cl_2, geminate recombination of the 17e radicals causes recovery of the bleaches for $[CpW(CO)_3]_2$ (labeled **A** in Figure 1). Note that the bleach centered at 1956 cm^{-1} overlaps with a peak from the 19e species (**C_1**), causing changes in this absorption at longer time delays (see the Supporting Information for details on the geminate recombination process). The primary reaction pathway of 17e radicals in phosphite solution is the formation of 19e intermediates. Correlation of the longer time constants for the decay of 17e and rise of 19e species in addition to the isosbestic points indicate that the 19e $CpW(CO)_3P(OMe)_3^{\bullet}$ (**C_1**) is generated from the 17e $CpW(CO)_3^{\bullet}$ (**B**) on a 400 ps time scale.

Disproportionation proceeds by the mechanism discussed in the Introduction and depicted in Scheme 2. Due to the extremely low concentration of $[CpW(CO)_3]_2$ in comparison to the other molecules, any mechanism involving this species (as in Scheme 1) can be ruled out on the picosecond time scale. In this particular sample, over 12 000 CH_2Cl_2 molecules and 1500 $P(OMe)_3$ molecules are present for every one $[CpW(CO)_3]_2$ molecule. Diffusional encounters of the 19e species with remaining $[CpW(CO)_3]_2$ molecules would not occur on the picosecond time scale. Furthermore, no evidence for the formation of $[CpW(CO)_3]_2^-$, an intermediate expected in the mechanism of Scheme 1, is observed in this experiment (see Table 1 for predicted frequencies of this species). The concentrations used in this study also indicate at least one $P(OMe)_3$ molecule will be present in the first solvation shell of the $[CpW(CO)_3]_2$ molecule prior to laser photolysis, allowing the formation of 19e species to easily occur within tens of picoseconds after laser photolysis.

The disproportionation mechanism of Scheme 2 is further supported by single-exponential fits to kinetic data, shown in Figure 2b, for $CpW(CO)_3^-$ (**E**) and $CpW(CO)_3P(OMe)_3^+$ (**D_1**), which yield time constants of 134 ± 27 and 140 ± 14 ps, respectively. The agreement of these time constants indicates that the disproportionated products are generated in a single kinetic event: electron transfer from $CpW(CO)_3P(OMe)_3^{\bullet}$ (**C_1**) to $CpW(CO)_3^{\bullet}$ (**B**) simultaneously forms the disproportionated products (**D_1**, **E**) as in Scheme 2. It is important to realize that this electron transfer reaction can only occur while the electron donor (**C_1**) and acceptor (**B**) species are in close proximity, a condition which is given only within the lifetime of the solvent cage. To understand cage effects on the extent and rate of disproportionation, we have studied the reaction in various concentrations of $P(OMe)_3$.

Cage Effects and Concentration Dependence. Changing the concentration of Lewis base $P(OMe)_3$ significantly alters the dynamics of all the reactive species. The results are summarized in Scheme 3. Homolysis of the dimer (**A**) produces two 17e radicals (**B**) enclosed by a cage of solvent molecules, represented by brackets. Coordination of a phosphite generates a 19e intermediate (**C_1**), and in all concentrations of $P(OMe)_3$, electron transfer between the solvent caged 17e (**B**) and 19e species (**C_1**) generates the disproportionated products (**D_1**, **E**). In low concentrations of $P(OMe)_3$, however, there is a competing process to disproportionation: separation of the radical species. As the solvent cage breaks down, the separation of the 17e and 19e species prevents electron transfer and hence prevents formation of the disproportionated products.

Time constants for all the reactive species at various concentrations of $P(OMe)_3$ are presented in Table 2. The formation times of the 19e intermediate are shorter with increasing $P(OMe)_3$ concentration; correspondingly, the decay of the 17e radical is faster. Note that the longer time constant for the decay of the 17e radical instead of the time constant for 19e intermediate formation has been used in our analysis of the concentration dependence as these two processes are correlated and the 17e transient absorptions exhibit lower noise.

(33) Since the disproportionation process consumes 19e species, the 19e dynamics in the first 150 ps might be expected to contain a component which directly corresponds to the disproportionation process. The 19e species, however, is also being formed from the 17e radical on this time scale and so no time component relating to disproportionation is necessarily expected. In addition, spectral overlap with the 17e radical peak prevents accurate analysis of the early time dynamics.

Table 2. Time Constants ($\tau = k^{-1}$) for Reactive Species in PR_3/CH_2Cl_2 Solutions of Varying Concentration[a]

		time constant (ps)				
R =	PR_3 concentration in CH_2Cl_2 (M)	$CpW(CO)_3^\bullet$ (17e, **B**)	$CpW(CO)_3PR_3^\bullet$ (19e, **C**)	$CpW(CO)_3PR_3^+$ (18e, **D**)	$CpW(CO)_3^-$ (18e, **E**)	$\frac{1}{2} \cdot \frac{\tau_{rad}}{\tau_{disp}}$ [b]
OMe	4.2	194 ± 25	174 ± 47	87 ± 12		1.11 ± 0.21
	3.6	199 ± 27	155 ± 43	114 ± 11		0.87 ± 0.15
	3.0	261 ± 7	276 ± 16[c]	121 ± 6		1.08 ± 0.06
	2.5	279 ± 18	307 ± 116[c]	139 ± 6	127 ± 13	1.00 ± 0.08
	2.0	363 ± 22	440 ± 26[c]	142 ± 11		1.28 ± 0.13
	1.6	417 ± 17	464 ± 101	140 ± 14	134 ± 27	1.49 ± 0.16
Bu	2.0	315 ± 5	353 ± 62	162 ± 13	138 ± 16	0.97 ± 0.08
	1.3	463 ± 25	508 ± 206	165 ± 15	160 ± 61	1.40 ± 0.15
Ph	2.0	213 ± 32		195 ± 28		0.55 ± 0.11
	1.6	229 ± 29		226 ± 16		0.51 ± 0.07
	1.3	221 ± 18		234 ± 16		0.47 ± 0.05

[a] Errors correspond to 95% confidence intervals; for the 17e and 19e species, values are the longer time component of a biexponential fit (see text). [b] Quotient of one-half of the time constant for $CpW(CO)_3^\bullet$ decay and time constant for $CpW(CO)_3PR_3^+$ formation (see text). [c] Calculated from Gaussian fits to the spectral data.[35]

The time constants for disproportionation initially increase as the concentration of $P(OMe)_3$ is lowered but then reach a plateau at concentrations of 2.5 M and lower.

To understand the observed behavior, the reactions occurring on a picosecond time scale must be analyzed in detail. Neglecting geminate recombination of the radicals, the two primary reactions are the reaction of 17e radicals with the Lewis base $P(OMe)_3$ to form 19e intermediates (1) and the reaction of 19e intermediates with 17e radicals to form the disproportionated products (2)

$$CpW(CO)_3^\bullet + P(OMe)_3 \underset{k_{-1}}{\overset{k_1}{\rightleftharpoons}} CpW(CO)_3P(OMe)_3^\bullet \quad (1)$$

$$CpW(CO)_3P(OMe)_3^\bullet + CpW(CO)_3^\bullet \xrightarrow{k_2} CpW(CO)_3P(OMe)_3^+ + CpW(CO)_3^- \quad (2)$$

Since near complete decay of the radical is observed in all phosphite solutions, the rate constant k_{-1} for dissociation of the 19e intermediates to 17e radicals and phosphite is assumed sufficiently small to be neglected in the following treatment of the kinetics. In-cage disproportionation (2) occurs on a fast time scale, exhibiting time constants below 150 ps in all cases. Since the 17e radical decay and 19e intermediate rise both occur on time scales approximately twice as long as disproportionation, the separation of time scales allows the 17e/19e dynamics to be modeled exclusively by reaction 1. Under pseudo first-order conditions, i.e., high $P(OMe)_3$ concentrations, the observed rate constant for (1), k_{obs}, depends linearly on the concentration of $P(OMe)_3$, with $k_{obs} = k_1[P(OMe)_3]$. A linear fit to the data is shown in Figure 3 and yields a value for the bimolecular rate constant of $k_1 = (1.1 \pm 0.2) \times 10^9\ M^{-1}s^{-1}$.

Understanding the concentration dependence of disproportionation is more complex. Both reactions 1 and 2 must be considered on time scales less than 150 ps. Since 19e intermediates are formed by reaction 1 but consumed by reaction 2, a steady-state approximation for 19e intermediates may be applied while (2) is sufficiently fast to maintain a low concentration of 19e species. While the steady-state assumption is not rigorously correct, it is sufficient to qualitatively interpret the experimental results. The rate of eqs 1 and 2 can be solved for the concentration of disproportionated product at time t

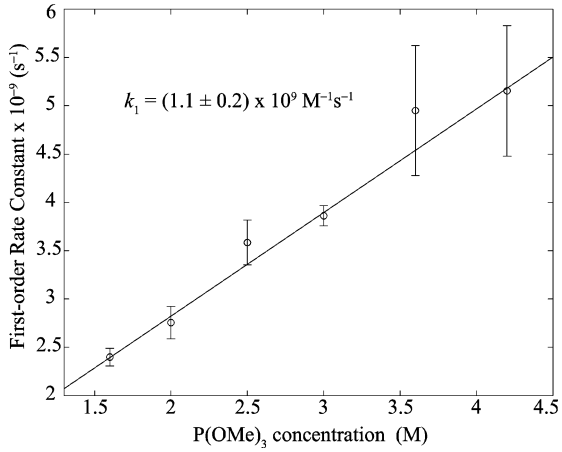

Figure 3. Dependence of the pseudo first-order rate constant for 19e intermediate formation on the concentration of Lewis base $P(OMe)_3$.

$$[CpW(CO)_3P(OMe)_3^+]_t = \frac{1}{2}[CpW(CO)_3^\bullet]_0(1 - e^{-2k_{obs}t}) \quad (3)$$

with $[CpW(CO)_3^\bullet]_0$ the initial concentration of the radical species. It can be shown that (3) implies the relationship $\tau_{disp} = 0.5 \times \tau_{rad}$, where τ_{disp} and τ_{rad} are the time constants for disproportionation and radical decay, respectively. Within errors, this relationship is valid for the four highest concentrations of $P(OMe)_3$, as illustrated by the quotient between one-half the time constant for the radical decay and the observed time constant for ultrafast disproportionation in Table 2. This quotient is close to unity for the four highest concentrations of $P(OMe)_3$, the expected result when the steady-state approximation and eq 3 are applicable. Since eq 3 depends on only one rate constant, k_{obs}, disproportionation is limited by the depletion of 17e radicals from reaction 1 rather than the electron transfer of reaction 2 in high Lewis base concentrations.

In the two lowest concentrations of $P(OMe)_3$ on the other hand, poor agreement with the steady-state prediction is observed, as indicated by the deviation from unity in the last column of Table 2. This discrepancy suggests that the steady-state approximation breaks down in lower concentration solutions and that the rate of electron transfer, k_2, becomes important. Studies on electron transfer in proteins and in electron donor and acceptor systems predict that the rate of electron transfer will decrease exponentially with the separation of the donor−

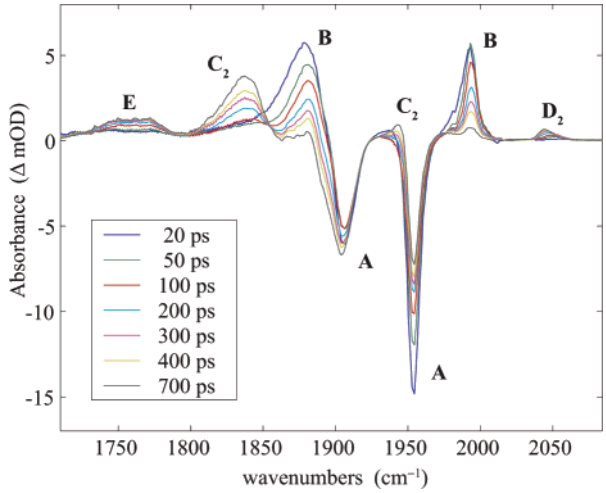

Figure 4. Transient difference spectra in the CO stretching region following 400 nm photolysis of $[CpW(CO)_3]_2$ in a 2.0 M solution of PBu_3 with CH_2Cl_2.

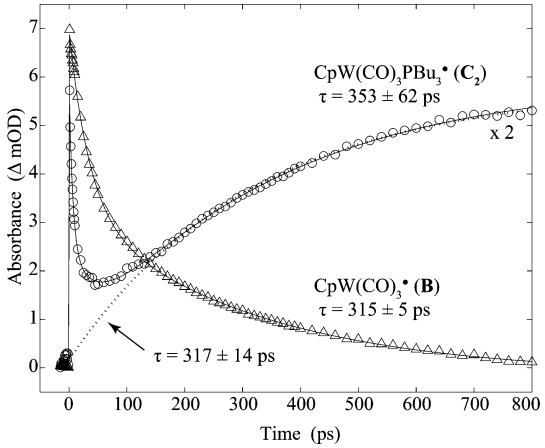

Figure 5. Kinetic plots for $CpW(CO)_3PBu_3^{\bullet}$ and $CpW(CO)_3^{\bullet}$ following 400 nm photolysis of $[CpW(CO)_3]_2$ in a 2.0 M solution of PBu_3 in CH_2Cl_2. Absorbance values for $CpW(CO)_3PBu_3^{\bullet}$ are scaled by a factor of 2 for clarity. Lines represent fits to the data (see text).

acceptor molecules.[36] In low $P(OMe)_3$ concentrations, therefore, separation of the radical pair may significantly slow electron transfer, limiting the rate of disproportionation. The separation of the radicals, equivalent to the breakdown of the solvent cage, can be viewed as a process which competes with disproportionation, as depicted in Scheme 3. The distance necessary to slow electron transfer can be estimated from the time constant for disproportionation. Treating the solvent as a viscous medium and using a random walk equation for three dimensions $x(\tau) = \sqrt{6D\tau}$ in neat CH_2Cl_2 with self-diffusion coefficient $D = 1.6 \times 10^{-6}$ cm^2/s, a time constant of $\tau = 140$ ps corresponds to a distance $x(\tau) = 3.7$ Å between two particles.[37] At distances above 3.7 Å, electron transfer may be sufficiently slow to kinetically limit the build-up of electron-transfer products.

Two regimes are apparent, as shown in Scheme 3. In the low concentration regime, diffusion limits the rate of disproportionation by separating the 17e electron acceptor and 19e electron donor. In the high concentration regime, disproportionation slows down due to depletion of the 17e radical population. The experimental results also suggest that increasing the $P(OMe)_3$ concentration increases the yield of disproportionated products on a picosecond time scale. A ratio of the $CpW(CO)_3PR_3^+$ peak intensity at 800 ps to the $[CpW(CO)_3]_2$ bleach intensity at 1 ps may provide a relative measure of the disproportionation yield. Although the data does not allow for a quantitative analysis, qualitatively, this ratio is observed to increase with higher $P(OMe)_3$ concentration. Raising the Lewis base concentration allows more electron-transfer events to occur before diffusional separation of the electron-transfer species, resulting in a greater yield of disproportionated products.

C. Reactions with PBu_3. The photochemistry of $[CpW(CO)_3]_2$ was also studied with the larger and more electron-donating Lewis base PBu_3. The results are qualitatively similar to those in phosphite solution, although the kinetics indicate that 19e formation is slightly faster with PBu_3. Figure 4 shows difference spectra of 1 mM $[CpW(CO)_3]_2$ in a 2.0 M solution of PBu_3 with CH_2Cl_2. The absorbances for $[CpW(CO)_3]_2$ (**A**) and 17e $CpW(CO)_3^{\bullet}$ (**B**) appear in the same positions as for other solutions (see Table 1). The 19e species $CpW(CO)_3PBu_3^{\bullet}$ (**C_2**) displays peaks at 1943 and 1836 cm^{-1}, in good agreement with DFT calculations contained in Table 1. The peak for $CpW(CO)_3PBu_3^+$ (**D_2**) is shifted from the corresponding peak of $CpW(CO)_3P(OMe)_3^+$ by 20 cm^{-1} to 2044 cm^{-1}, also in accord with the prediction from DFT calculations (17 cm^{-1}). $CpW(CO)_3^-$ (**E**) is resolved into two separate bands at 1751 and 1771 cm^{-1}, most likely due to polarity effects from the countercation.[14]

As in phosphite solution, an isosbestic point at 1855 cm^{-1} in Figure 4 indicates that the 19e intermediate (**C_2**) is formed from the 17e radical (**B**). Kinetic fits to the data support this conclusion and are shown in Figure 5. Due to the greater separation between the 17e and 19e peaks, the kinetic data with PBu_3 exhibit less noise than those obtained for phosphite solution. Kinetics for $CpW(CO)_3^{\bullet}$ (**B**) were fit to two exponential decays, yielding time constants of 35 ± 2 and 315 ± 5 ps. The fast decay results from a combination of vibrational relaxation, disproportionation, and geminate recombination while the longer decay results from the formation of 19e intermediates. Kinetics for the 19e $CpW(CO)_3PBu_3^{\bullet}$ (**C_2**), also shown in Figure 5, were fit to two exponential decays and one exponential rise, giving time constants of 6 ± 1, 43 ± 14, and 353 ± 62 ps, respectively. The decays result from overlap with the vibrationally hot and red shifted 17e radical absorbance while the exponential rise is attributed to the formation of 19e intermediates.[33] Figure 5 also shows a single-exponential fit (dotted line) to the 19e kinetic data omitting all points between 0 and 50 ps, which are dominated by vibrational relaxation of the 17e radical species. This fit yields a time constant of 317 ± 14 ps for the rise of the 19e species, in excellent agreement with the decay time of the 17e radical (315 ± 5 ps). Fits to the kinetic data for the disproportionated products (not shown) yield time constants of 162 ± 13 ps for $CpW(CO)_3PBu_3^+$ and 138 ± 16 ps for $CpW(CO)_3^-$. As in phosphite solution, the disproportionated products are formed in the same kinetic event: in-cage electron transfer between the 17e and 19e species (see Scheme 2).

Data were obtained at two concentrations of PBu_3 (see Table 2) and suggest that the same regimes and cage-effects discussed for phosphite solutions are also true for PBu_3. The quotient in

(34) Scott, A. P.; Radom, L. *J. Phys. Chem.* **1996**, *100*, 16502−16513.
(35) The spectral data between 100 and 800 ps was fit to multiple Gaussian functions and the area of peaks corresponding to the 19e intermediate at multiple time delays were fit to a monoexponential rise, yielding the time constants cited.
(36) Barbara, P. F.; Meyer, T. J.; Ratner, M. A. *J. Phys. Chem.* **1996**, *100*, 13148−13168.
(37) Yu, Y.-X.; Gao, G.-H. *Fluid Phase Equil.* **1999**, *166*, 111−124.

Scheme 4. Reaction of $[CpW(CO)_3]_2$ with PPh_3[a]

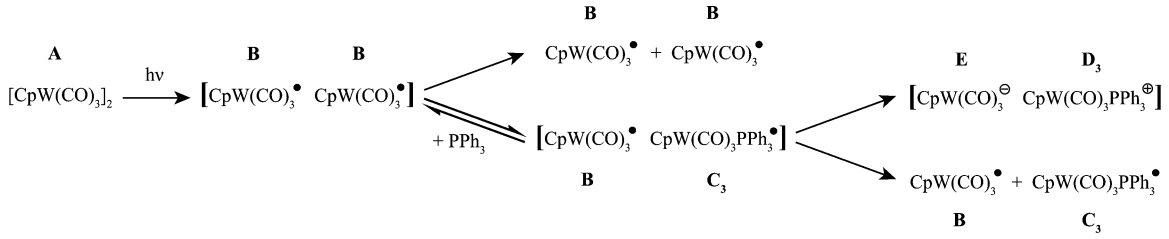

[a] Brackets represent the solvent cage.

the last column of Table 2 indicates that in a 1.3 M concentration of PBu_3 disproportionation is limited by separation of the caged radical pair (low concentration regime) while at a 2.0 M concentration disproportionation is limited by the depletion of the 17e radical population (high concentration regime). Unfortunately, due to decreasing solubility of $[CpW(CO)_3]_2$ with high concentrations of PBu_3, reliable data above a 2.0 M concentration were not obtained. Data at a 1.6 M PBu_3 concentration were not acquired due to difficulties in handling the pyrrophoric Lewis base, but results at this concentration would almost certainly lie between those observed at a 1.3 and 2.0 M concentration and not alter the discussion. Applying the same pseudo first-order rate expression for the formation of 19e species used with phosphite solutions, $k_{obs} = k_1[PBu_3]$, the kinetic data at the two concentrations yield a rate constant of $k_1 = (1.5 \pm 0.3) \times 10^9\ M^{-1}s^{-1}$ for the formation of the 19e intermediate $CpW(CO)_3PBu_3^\bullet$ from the 17e radical $CpW(CO)_3^\bullet$.

D. Reactions with PPh_3. In comparison to $P(OMe)_3$ and PBu_3, significant formation of the 19e intermediate is *not* observed in reactions with PPh_3, yet ultrafast disproportionation still occurs to a significant extent. The reactions occurring with PPh_3 are summarized in Scheme 4. Photolysis generates the solvent caged 17e radicals (**B**) and equilibrium between the 17e radical and 19e intermediate (**C_3**) is established. This 17e/19e equilibrium favors 17e species, allowing a significant portion of the 17e radicals to escape the solvent cage without reacting. Of the portion which do form 19e intermediates, electron transfer may generate the disproportionated products (**D_3**, **E**) or the 17e and 19e pair may escape the solvent cage.

Figure 6 shows transient difference spectra collected in PPh_3. Absorptions for the parent dimer (**A**) and 17e radicals (**B**) appear at the same positions as with the other Lewis bases, but peaks for the 19e species (**C_3**) and disproportionated cation (**D_3**) are shifted to approximately 1850 and 2054 cm^{-1}, respectively. These peak positions are in good agreement with the frequencies obtained from DFT calculations (see Table 1). Only one peak for the 19e species (**C_3**) is apparent in the spectra, most likely due to spectral overlap of the second peak with the strong bleach at 1956 cm^{-1}.[38] Figure 7 shows kinetic plots for the 17e radical (**B**) and one disproportionated product (**D_3**). In contrast to $P(OMe)_3$ and PBu_3, the long time component measured for 17e radical decay (**B**) matches the rise time for the disproportionated product (**D_3**) within errors. This agreement suggests that the decay of the 17e radical results from electron transfer to the disproportionated products and preservation of 17e/19e equilibrium rather than the formation of 19e intermediates outside the solvent cage.[40] The dynamics were observed at various concentrations of PPh_3 (see Table 2) and in all cases the 17e radical did not decay completely.

Formation times for disproportionated products in PPh_3 show no significant concentration dependence (see Table 2), which is consistent with the results for $P(OMe)_3$ at similar concentrations. As already discussed, the build-up of disproportionated products can either be limited by the separation of solvent-caged radicals or the depletion of 17e radical population. In the latter case, a strong concentration dependence should be apparent. If, on the other hand, the separation of 17e radicals limits the build-up of disproportionated products, then little concentration dependence would be expected.[41] The lack of concentration dependence in the experimental data suggests that the rate-

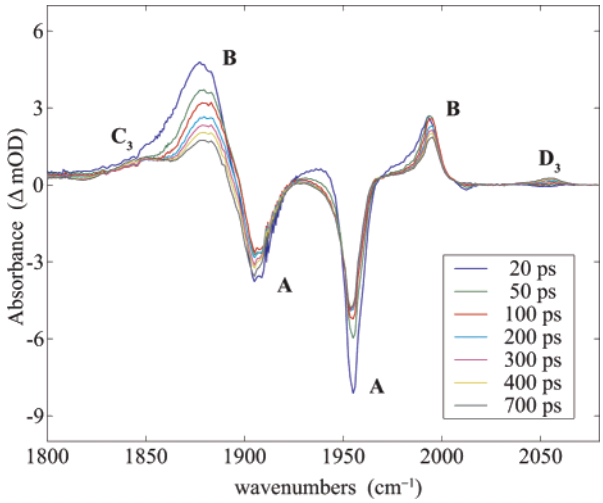

Figure 6. Transient difference spectra in the CO stretching region following 400 nm photolysis of $[CpW(CO)_3]_2$ in a 1.3 M solution of PPh_3 in CH_2Cl_2.

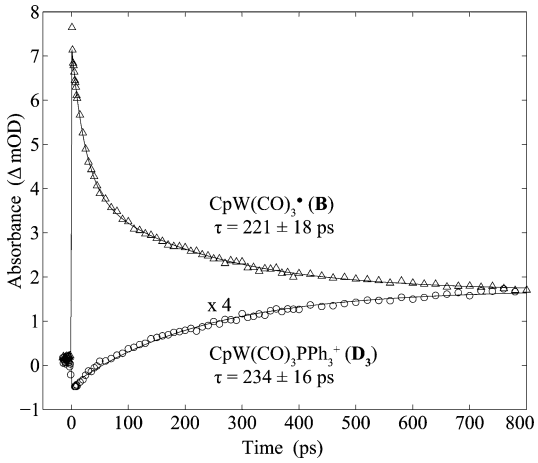

Figure 7. Kinetic plots for $CpW(CO)_3^\bullet$ and $CpW(CO)_3PPh_3^+$ following 400 nm photolysis of $[CpW(CO)_3]_2$ in a 1.3 M solution of PPh_3 in CH_2Cl_2.[39] Lines represent fits to the data (see text).

(38) Unfortunately, PPh_3 is on the edge of a π to π^* transition at the excitation wavelength of 400 nm, causing absorption of the pump light by the solvent and a lower signal-to-noise ratio. As a result, no reliable data could be recorded below 1800 cm^{-1} where $CpW(CO)_3^-$ is expected to absorb.

limiting process for ultrafast disproportionation in PPh_3 at the concentrations used in this experiment is the separation of caged radicals rather than the depletion of 17e, electron acceptor species.

As apparent from Figure 6, the peak from the 19e species (**C_3**) is less intense in comparison to the other Lewis bases and rather than growing in, maintains an almost constant intensity after vibrational cooling of the highly overlapped 17e radical peak (**B**). These observations suggest that the 19e $CpW(CO)_3PPh_3^{\bullet}$ is less stable than its counterparts in other Lewis bases and that the 17e/19e equilibrium favors 17e species, consistent with Scott and co-workers estimate of only $K = 6 \pm 1$ L·mol^{-1} as the equilibrium constant ($K = k_1/k_{-1}$) for the process.[12] It is plausible to assume that while species in solution are vibrationally excited the reactants are able to overcome the barrier to 19e intermediate formation and reach the equilibrium concentration for the species within tens of picoseconds. No additional formation of the 19e species is observed on the picosecond time scale, so the decay of the 17e radical results exclusively from the disproportionation process,[40] explaining the correlation of the two respective time constants. Since the 17e/19e equilibrium favors 17e radicals, both species should be present on longer time scales and thus may react out-of-cage. Experiments to understand the reactions on diffusion-limited time scales are currently in progress.

It is interesting to note that the 19e peak displays negligible growth while the 17e peak is still decaying. This observation might indicate that the 19e species is not an intermediate for disproportionation and that an inner sphere mechanism for electron transfer may occur. In this case, the reaction would proceed directly from the caged 17e radicals to the disproportionated products, with the coordination of a Lewis base occurring concurrently with electron transfer. In comparison, an outer sphere mechanism would first require formation of the 19e species and then transfer of the electron, as depicted in Scheme 2. The current experimental data does not distinguish between an inner sphere mechanism without formation of 19e intermediates and an outer sphere mechanism in which electron transfer is sufficiently fast to prevent the build-up of the 19e species. Further experimental and theoretical investigations in this direction are in progress in our laboratories.

E. Comparison of the Reactivity in Different Lewis Bases. Steric and Electronic Effects. The stability and reactivity of $18+\delta$ compounds is affected by the nature of the organometallic fragment, coordinating ligand, and solvent. The organometallic species and solvent were the same in all experiments conducted, so differences in chemical dynamics result solely from the different properties of the three coordinating ligands (PR_3; R = OMe, Bu, Ph). A low energy π^* orbital in the coordinating ligand tends to enhance the stability of $18+\delta$ compounds since the '19th' electron can localize in the antibonding orbital rather than occupying a higher energy metal-centered orbital.[4,5] Reduction potentials of the lone ligand are correlated with the ligand's ability to stabilize $18+\delta$ compounds by accommodating the extra electron in a vacant molecular orbital.[5,42] A more positive reduction potential approximately indicates a smaller HOMO/LUMO energy gap and corresponds to more stable $18+\delta$ compounds but decreased reactivity toward electron transfer.[5] In the absence of reduction potentials for the ligands themselves,[43] the reduction potentials ($E°$) for $CpFe(CO)(COMe)PR_3^+$ will be used to establish the trend for the PR_3 ligands. Reduction potentials for the $CpFe(CO)(COMe)PR_3^{+/0}$ couple were measured relative to acetylferrocene at 20 °C and for the three relevant ligands it was found that $P(OMe)_3$ (−0.1344 V) > PPh_3 (−0.2630 V) > PBu_3 (−0.3990 V).[44] In addition to orbital considerations, electron-donating ability and cone-angle are two prototypical ligand properties which may affect the stability and reactivity of 19e intermediates. Cone-angle is the generally accepted measure of the size of coordinating ligands,[45] with PPh_3 (145°) > PBu_3 (132°) > $P(OMe)_3$ (107°).[14] The electron donating ability of phosphine and phosphite ligands can be measured by the a_1 mode CO stretching frequencies of $Ni(CO)_3L$ (L = phosphine or phosphite). Due to CO π back-bonding, lower frequencies correspond with better electron donating ability; hence, in terms of relative electron-donating ability PBu_3 (2060.3 cm^{-1}) > PPh_3 (2068.9 cm^{-1}) > $P(OMe)_3$ (2079.5 cm^{-1}).[46] These three ligand properties, reduction potential, cone-angle, and electron donating ability, control the stability of 19e species and can be used to understand the observed reactivity.

The Lewis bases $P(OMe)_3$ and PBu_3 produce qualitatively similar results, while PPh_3 exhibits significantly different behavior. 19e intermediates form to a smaller extent and on a different time scale in the presence of PPh_3, which lies between the other two ligands in terms of both electron-donating ability and reduction potential. Neither of these properties appears to be the determining factor for the kinetics and extent of 19e intermediate formation with PPh_3. Instead, the cone-angle, which indicates that PPh_3 is the largest of the three Lewis bases (145°), is best correlated with the experimental data and implies that steric effects hinder the formation of a 19e species with PPh_3. The cone-angles of $P(OMe)_3$ and PBu_3 are smaller than PPh_3 yet significantly different from one another at 107° and 132°, respectively. Despite this difference of 25°, the experimental results in $P(OMe)_3$ and PBu_3 are qualitatively similar, suggesting that cone-angles only become important when the steric hindrance exceeds a certain limiting value (here between 132° and 145°). This observation is in agreement with a study by Tyler in which a sudden change in reactivity was found between PPh_2Bu_3 (140°) and PPh_3 (145°).[14]

Quantitative analysis of the results in $P(OMe)_3$ and PBu_3 suggests that the formation of 19e species is slightly faster in PBu_3, with a rate constant of $(1.5 \pm 0.3) \times 10^9$ M^{-1}s^{-1} in comparison to $(1.1 \pm 0.2) \times 10^9$ M^{-1}s^{-1} for $P(OMe)_3$. The calculated rate constants may not be rigorously distinguishable, but the opposite trend would be expected if steric factors played

(39) The kinetic trace for $CpW(CO)_3PPh_3^+$ begins at a negative absorbance value due to a weak bleach resulting from build-up of this product in the solution. This bleach appears after very short periods of laser photolysis most likely due to a very high quantum yield for disproportionation at high concentrations of PPh_3.

(40) A similar decay should be present with $P(OMe)_3$ and PBu_3, but it is sufficiently low in amplitude to be masked by the larger decay resulting from 19e formation in these Lewis bases.

(41) Changes in concentration alter diffusion coefficients for solutions, changing the rate of diffusion. For small concentration differences, changes in the diffusion coefficient should be negligible.

(42) Lacoste, M.; Astruc, D. *J. Chem. Soc., Chem. Commun.* **1987**, 667−669. Lacoste, M.; Rabaa, H.; Astruc, D.; LeBeuze, A.; Saillard, J.-Y.; Précigoux, G., *Organometallics* **1989**, *8*, 2233−2242.

(43) To the best of our knowledge, these values have not been published. Initial attempts to determine the reduction potentials of the phosphines suggest that decomposition of the solvent may occur before reduction is achieved; however, more rigorous attempts are called for.

(44) Fernandez, A. L.; Ying Lee, T.; Reyes, C.; Prock, A.; Giering, W. P., *Organometallics* **1998**, *17*, 3169−3175.

(45) Tolman, C. A. *Chem. Rev.* **1977**, *77*, 313−348.

(46) Tolman, C. A. *J. Am. Chem. Soc.* **1970**, *92*, 2953−2956.

Table 3. Charges (in atomic units) of Molecular Fragments in the 17e $CpW(CO)_3^•$ and 19e $CpW(CO)_3PR_3^•$ (R = OMe, Bu, Ph) Complexes and Average CO Bond Lengths

	$CpW(CO)_3^•$ (**B**)	$CpW(CO)_3P(OMe)_3^•$ (C_1)	$CpW(CO)_3PBu_3^•$ (C_2)	$CpW(CO)_3PPh_3^•$ (C_3)
q(W)	0.0197	−0.3529	−0.3078	−0.3152
1/3 $q((CO)_3)$	0.0472	0.0332	−0.0168	0.0076
$q(W(CO)_3)$	0.1613	−0.2530	−0.3582	−0.2923
q(Cp)	−0.1613	−0.1556	−0.1621	−0.1375
$q(CpW(CO)_3)$	0	−0.4086	−0.5203	−0.4298
$q(PR_3)$		0.4086	0.5203	0.4298
r(CO)/Å	1.163	1.168	1.172	1.169

an important role in the formation of 19e intermediates with these Lewis bases. Instead, electronic parameters appear important when the steric hindrance is below a certain limiting value. The reduction potential and electron-donating ability of PBu_3 indicate that it is less likely to accept extra electron density into a vacant molecular orbital and more likely to donate electron density to the metal center in comparison to $P(OMe)_3$. Upon the basis of the experimental data, these two properties enhance the rate of 19e intermediate formation when steric effects are no longer an important consideration. The enhanced rate of 19e formation also causes the high concentration regime in PBu_3 to be achieved at a lower concentration (2.0 M) than was observed with $P(OMe)_3$ (2.5 M; see last column of Table 2).

In the low concentration limit of the three Lewis bases, the differences observed in the time constants for disproportionation between the Lewis bases (Table 2) may be attributed to differences in the respective viscosity and diffusion constants of these solutions. Disproportionation in PPh_3, however, occurs for a significantly longer period of time in comparison to the two smaller Lewis bases. In addition to viscosity and diffusion considerations, PPh_3 may facilitate electron transfer better than the other Lewis bases, contributing to the longer period of disproportionation. The details of this electron-transfer process, as well as the 17e/19e equilibrium, are currently under investigation and will be discussed in a future publication.[26]

Atomic Charge Distributions. Calculations on charge distributions in the 17e and 19e complexes were carried out to elucidate the experimental results. Data from the NBO analysis are reported in Table 3. The charges on the PR_3 ligand and W atom in the $CpW(CO)_3PPh_3^•$ complex lie between the values for the other two Lewis bases, supporting our conclusion that steric rather than electronic effects dominate the behavior of PPh_3.

The charges of the PR_3 ligands in the 19e $CpW(CO)_3PR_3^•$ complexes become more positive in the order $P(OMe)_3$ < PPh_3 < PBu_3, in agreement with the trends in electron-donating ability and reduction potential quoted above. Because the 19e complex is neutral, the charge on the PR_3 ligand is exactly balanced by a negative charge on the $CpW(CO)_3^•$ portion of the species and the Cp moiety bears a considerable fraction (about one-third) of this negative charge. Since the q(Cp) values are comparable for the three 19e complexes (see Table 3), the charges on the $W(CO)_3$ unit correspond to the aforementioned trend, with the R = Bu complex exhibiting the greatest negative charge. Within the $W(CO)_3$ unit, however, the most negatively charged W atom is, surprisingly, in the R = OMe complex. This result may explain why 19e intermediate formation in $P(OMe)_3$ is slightly slower in comparison to PBu_3. The average charges on the CO molecules are positive for the R = OMe complex and negative for the R = Bu complex, while the R = Ph species contains, on average, almost neutral CO ligands. Note that these are average values, and the individual CO values show different charges (even different in sign). The 19th electron is mostly localized in antibonding orbitals,[2] rendering the average CO bond lengths relatively long. Accordingly, the frequencies become smaller, in agreement with experiment (see Table 1).

There is still a conceptual problem concerning whether the 19e intermediates are true 19e species or should rather be classified as 18+δ complexes. Several definitions of δ can be found in the literature. In one theoretical study, δ is calculated as the difference in charge on ligands in cationic 18e and neutral 19e complexes.[47] Alternatively, δ can be understood in terms of the spin density, or more exactly the unpaired electron density, localized on the metal center.[8,48] The results of similar calculations as well as a more detailed discussion of the atomic charge results will be presented in a forthcoming publication.[26] Here, we use $\delta = q(W)$ as a meaningful definition that would yield δ values of about one-third of an elementary charge.

IV. Summary and Conclusion

The complex dynamics of 19e intermediate formation and disproportionation following 400 nm photolysis of $[CpW(CO)_3]_2$ in the presence of Lewis bases PR_3 (R = OMe, Bu, Ph) have been resolved on a picosecond time scale, and the results are summarized in Scheme 5.[49] The dynamics depend on both the identity and concentration of Lewis base, with the results separating into three distinct categories: **(I)** $P(OMe)_3$ and PBu_3 at high concentration, **(II)** $P(OMe)_3$ and PBu_3 at low concentration, and **(III)** PPh_3. In all cases, photolysis initially results in the formation of solvent caged 17e $CpW(CO)_3^•$ radicals (the brackets in Scheme 5 represent the solvent cage). Coordination of a Lewis base with one 17e radical forms a 19e intermediate $CpW(CO)_3PR_3^•$, with the equilibrium favoring 19e species in the order Bu > OMe ≫ Ph. In all cases, disproportionation to the 18e $CpW(CO)_3^-$ and $CpW(CO)_3PR_3^+$ occurs by transfer of an electron from a 19e to 17e species within the same solvent cage.

For case **I**, disproportionation ceases due to the decrease in 17e radical (electron acceptor) population. In cases **II** and **III** on the other hand, disproportionation ceases due to diffusional separation of the caged radical pair.[49] Once the electron donor and acceptor have separated by several angstroms, electron transfer is sufficiently slow to limit the build-up of dispropor-

(47) Srinivas, G. N.; Yu, L.; Schwartz, M. *J. Organomet. Chem.* **2003**, *677*, 96−100.
(48) Braden, D. A.; Tyler, D. R., *J. Am. Chem. Soc.* **1998**, *120*, 942−947.
(49) Neglected in Scheme 5 are reactions involving separation of the 17e radicals prior to 19e formation. This scenario likely occurs for cases **II** and **III** and to a lesser extent for **I**. For cases **II** and **III**, 17e radical separation prevents disproportionation in the same manner as separation of the 17e and 19e species.

Scheme 5. Proposed Mechanisms for 19e Intermediate Formation and Disproportionation in Lewis Bases PR_3 (R = OMe, Bu, Ph) at Varying Concentrations in CH_2Cl_2[a]

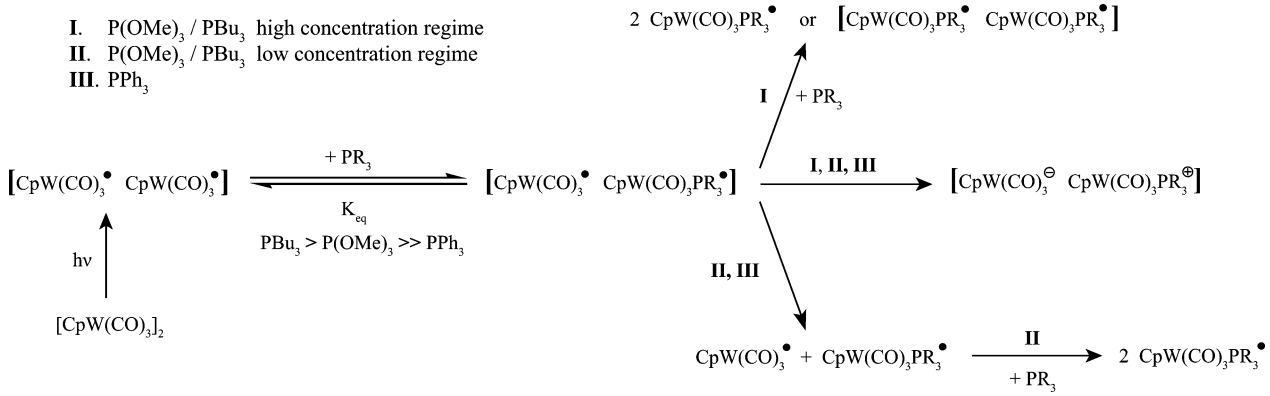

[a] Brackets represent the solvent cage. Reactions in which both caged 17e radicals only react following breakdown of the solvent cage are omitted for clarity.[49]

tionated products. The longest period of disproportionation is observed in case **III** (PPh_3), suggesting that PPh_3 facilitates electron over a longer separation than the other two Lewis bases.

In cases **I** and **II** ($P(OMe)_3$ and PBu_3), the equilibrium favors 19e species, so nearly all the 17e radicals not consumed by the in-cage disproportionation reaction are converted to 19e species, as shown in Scheme 5. The rate of 19e formation is slightly faster with PBu_3, an effect best attributed to the electronic properties (e.g., greater electron-donating ability) of this Lewis base. With PPh_3 (case **III**) on the other hand, the 17e/19e equilibrium favors the 17e radical, so only limited formation of a 19e species is observed. The behavior of PPh_3 is attributed to steric rather than electronic effects since its electronic parameters (electron-donating ability, reduction potential, atomic charges) lie between the other two Lewis bases. The results with the three Lewis bases indicate that steric hindrance dominates the 19e dynamics when the cone-angle of the Lewis base exceeds a certain limiting value while electronic effects dominate below this limiting value (between 132° and 145°). The details of 17e/19e equilibrium as well as the electron-transfer process are still under investigation and will be presented in a forthcoming publication.[26]

The presence of the three categories (**I**, **II**, **III**) cited above provide the opportunity to manipulate the extent of ultrafast disproportionation by controlling the concentration and identity of the Lewis base. Other chemical processes, such as CO ligand substitution,[50] may compete with disproportionation on longer, diffusion-limited time scales (nanosecond to milliseconds). In such a case, the primary mechanism for disproportionation may be the one proposed here, while different processes involving the 19e species occur on longer time scales. As a result, the extent of disproportionation in comparison to other processes may be affected by the identity of Lewis base and potentially controlled with the concentration. The results with different concentrations of $P(OMe)_3$ suggest that the yield of disproportionated products on a picosecond time scale increases with increasing $P(OMe)_3$ concentration since more electron-transfer events can occur before the electron donor and acceptor are separated.[51]

This paper confirms the formation of highly reactive 19-electron species and describes a mechanism for disproportionation by in-cage electron transfer between a 17e and 19e species. In this study, disproportionation is complete within ca. 200 ps, yet the 17e and 19e species both persist beyond the time scale of the experiment (800 ps). The reactions of these radicals on longer time scales is still an unresolved question. For instance, the disproportionation mechanism proposed by Tyler (Scheme 1) is appropriate on diffusion-limited time scales (nanoseconds to milliseconds) yet has not been directly observed using time-resolved IR spectroscopy. Experiments designed to probe the dynamics on longer time scales and distinguish the different mechanisms or processes involved in the radical chemistry are currently in progress.

Acknowledgment. We thank the National Science Foundation (NSF) for funding and the Office of Basic Energy Sciences, Chemical Sciences Division, of the U.S. Department of Energy under contract DE-AC03-76SF00098 for the use of some specialized equipment. J.F.C. acknowledges support through an NSF graduate research fellowship, M.F.K. is grateful for support by the Alexander von Humboldt foundation through a Feodor-Lynen Fellowship, and S.S. thanks the Fonds der Chemischen Industrie for financial support. We also thank Prof. Hermann Stoll (University of Stuttgart) for fruitful discussions.

Supporting Information Available: Details on the geminate recombination process and complete ref 20. This material is available free of charge via the Internet at http://pubs.acs.org.

JA052221G

(50) Turaki, N. N.; Huggins, J. M. *Organometallics* **1986**, *5*, 1703−1706.

(51) At extremely high concentrations (e.g., with the Lewis base as solvent) the formation of two 19e species within the same solvent cage may hinder disproportionation.